Energy Reports 5 (2019) 136–144

Contents lists available at ScienceDirect

Energy Reports

journal homepage: www.elsevier.com/locate/egyr

Research paper

Development of a robust nonlinear pitch angle controller for a redesigned 5MW wind turbine blade tip

Ranjeet Agarwala

Department of Technology Systems, College of Engineering and Technology, East Carolina University, Greenville, NC, 27858, USA

ARTICLE INFO

Article history:
Received 4 October 2018
Received in revised form 12 December 2018
Accepted 27 December 2018
Available online 23 January 2019

Keywords:
Renewable energy
Wind energy
Wind turbine
Control
Sliding mode control
Robust control

ABSTRACT

Power in wind turbines are traditionally controlled by varying the pitch angle at high wind speeds in region 3 of the wind turbine operation. The pitch angles controllers are normally driven by electrical or hydraulic actuators. The motivation of this research is to design and implement a pitch angle control strategy at the outer section of the blade via a separated pitch control at blade tip (SePCaT). A pneumatic actuator is implemented to drive the pitch angle control mechanism by incorporating pneumatic actuated muscles (PAM) due to its high power/mass ratio, high specific work, and good contraction ratio while maintaining low weight at the tip of the blade. A sliding mode controller (SMC) is modeled and implemented on a redesigned 5MW wind turbine numerically. The hypothesis is that the SePCaT control strategy is effective and satisfactory pitch angle trajectory tracking is achievable. The method is adopted, the system is modeled, and the response was observed by subjecting the model dynamics to desired pitch angle trajectories. Initially comparative controller response with respect to desired trajectory revealed satisfactory pitch angle tracking but further investigation revealed chattering characteristics which was minimized by incorporating a saturation function. SePCaT offers an effective pitch angle control strategy which is smaller, lighter, reliable and efficient.

1. Introduction

The remarkable growth in the wind energy sector poses challenges on many fronts as the rotor sizes and tower heights continue to grow to accommodate larger land based and offshore wind turbine capacities. One of the challenges is controlling large wind turbine rotors at high wind speeds. In large wind turbines and at high wind speeds, rated power output is maintained by controlling the blades pitch angle at the root of the blade. Actuations of pitch angle due to wind variations can lead to significant fluctuations in wind turbine blade loads affecting rated turbine power output, stability, and turbine life. This is particularly pronounced in region 3 of the wind turbine operation where the pitch angle is varied to abate power so that the wind turbine is not subject to high aerodynamic and operation stresses. Region 3 is commonly referred to area of the wind power-wind velocity curve where high wind speeds produce more than the rated power for a specific wind turbine. The blades are generally pitched to feather (pitch angle is reduced) to shed the excessive power by feathering the blades (reducing the angle of attack) individually or collectively. Feathering blades at high speeds are inhibited by high blade inertia leading to slower control response time at high or fluctuating speeds. Power required for full length pitching for large blades are high thereby undermining power generation. Mechanisms for full length pitching are large, complex, and expensive requiring higher manufacturing and maintenance costs. This problem is further compounded by the randomness and uncertainties in wind speed which introduces nonlinearities in blade aerodynamics and causes complexities in controlling large wind turbine blades. Therefore, as wind turbines continue to grow and achieve power ratings to the order of around 20 MW capacities, independent or collective full-length pitch control become increasingly cumbersome.

Wind turbine system is highly nonlinear due to unmolded dynamics, model dynamic coupling and input variations. Randomness and uncertainties in wind speed introduce nonlinearities in blade aerodynamics which introduces complexities. Due to this non-linearities, SMCs are becoming more prevalent compared to traditional controller such as Proportional, Integral, and Derivative (PID) Controllers. Many researchers have shown that SMC controllers exhibit high robustness in controlling wind turbine systems. Hu and his colleagues (Hu et al., 2017) have shown that a sliding mode controller improves the performance of the wind turbine system under system uncertainties and external disturbances. Yang et al. (2018b,a) and his colleagues implemented robust sliding-mode control of wind energy conversion systems for optimal power extraction via nonlinear perturbation observers. Yin et al. (2015c) proposed a state-of-the-art sliding mode and fuzzy logic based maximum power point tracking control for the wind turbine. The novel DC-side voltage controller exhibited low

E-mail address: agarwalar@ecu.edu.

https://doi.org/10.1016/j.egyr.2018.12.005

steady-state error and the ability to track optimum rotor angular velocity and generator power when compared with traditional approaches. The proposed controller offers a simple, flexible, and easily implemented solution for practical wind energy systems. Yin and his colleagues (Yin et al., 2015e) focused on the design of a pitch angle control system wherein a hydraulic motor was used to enhance the power/mass ratio of a traditionally used electromechanical pitch system. They reported that the accuracy of the control was improved by replacing the slider-crank mechanism with a rotary hydraulic servo. The pitch angle control system exhibited high power/mass ratio and precision. The pitch control system was appropriate for industrial and field use as it offered superior performance improvements with regards to trajectory tracking. Deployment of this pitch control system enabled abatement of output power and drive torque fluctuations with high reliability.

Yin et al. (2015d) designed an innovative wind turbine controller for maximizing power and eliminating voltage harmonics at the generator. Their system which comprised of a fuzzy sliding mode voltage controller was purposed for a direct-driven wind energy system with a three-phase bridge rectifier. A harmonic compensator was included in the fuzzy logic generator to eliminate the harmonics at the generator. The controller facilitates optimum DC-side current to be inferred from current and voltage variations thereby enabling maximum energy capture with high accuracy and efficiency.

Yin and his colleagues (Yin et al., 2014b) designed a control strategy for a hydro-viscous transmission based continuously variable speed wind turbine. The system is based on a particle swarm optimization algorithm based multi-objective optimization method to augment the efficiency of transmission. The hybrid output power control system smoothens and abates power and torque fluctuations effectively. Yin and his colleagues (Yin et al., 2015f) proposed pitch control system controlled by a variable-displacement pump and enabled by an adaptive sliding mode back-stepping control algorithm. The components included a variable-displacement hydraulic pump, a fixed-displacement hydraulic motor, and a gear set. The system was designed to follow the pitch angle trajectory under the presence of external disturbances and uncertainties and the accuracy and stability is guaranteed by Lyapunov algorithm. The pitch angle control mechanism has significant advantages such as high operating efficiency, high energy-savings capability, high torque to weigh ratio and compactness. This makes the system suitable for field deployment when compared to a valve-controlled pitch system enabling reduction of generator power fluctuations and reduction of flap-wise load. Yin and his colleagues (Yin et al., 2015g) designed a fuzzy logic sliding-mode control strategy to optimize energy capture and abate current harmonics in the generator area. The hybrid system comprised of a fuzzy logic controller and a double integral sliding-mode current controller to optimally track dc-current, and a resonant filter to abate generator-side current harmonics. The system facilitated sensorless maximum power point tracking (MPPT) control effectively with high accuracy. Yin and his colleagues (Yin et al., 2014a) proposed a pitch control system for a wind turbine wherein the system is actuated by a servo-valve controlled hydraulic motor and the control algorithm is enabled by an adaptive nonlinear sliding mode to deal with system uncertainties and external disturbances. The pitch control system was accurate and efficient and performed reliably and demonstrated superior performance capabilities with regards to reduction improvements in external load and tower top vibrations when compared to collective pitch control. Yin and his colleagues (Yin et al., 2015b) designed an electro-hydraulic pitch system suitable for mid to large wind turbines that is enabled and actuated by a servo-valve hydraulic motor and is modeled in state space representation incorporating parametric uncertainties and non-linearities. The system had improved performance due to low friction realized by low sped hydraulic motor and a simple gear set design. Desired pitch trajectory tracking along with output power and drive-train torque fluctuation abatement is achieved in the presence of model uncertainties and external disturbances by adopting an adaptive back-stepping control algorithm. The pitch control system exhibited superior performance when compared to traditional controllers and offered better accuracy, affordability and energy efficacy enabling high power density when compared to exclusively electrically actuated pitch system. Yin et al. (2016b) designed a direct drive-train speed control system to augment the wind turbine controllability and reliability and incorporated a hydro-viscous transmission. The system incorporated a fixed gear ratio ad continually adapted to the incoming wind speed and maintained optimized power points as evidenced by numerical results on a 2.0 MW wind turbine. Yin and his colleagues (Yin et al., 2016a) proposed an innovative electro-hydraulic digital servo system (EDSS) digitally enabled predictive pitch control system. The system regulated the pitch angle accurately with fast response time. The power to mass ratio of the system was low due to the deployment of hydraulic axial piston motor. The system utilized an extreme learning machine (ELM) based on online training that approximated the wind turbine characteristics that were nonlinear offering high effectiveness, fast learning capabilities, and abatement of output power and drive-train torque fluctuation. Yin and his colleagues (Yin et al., 2015) designed and improved a wind turbine simulator for steady state and dynamic and reproduced five-degree-of-freedom turbine loads. The improved simulator overcame the drawbacks of the current system by representing rotor and blades by rotating disc to emulate inertia effects and by incorporating twenty-four electro-hydraulic loading actuators symmetrically distributed around the rotating disc and controlled independently. A loading decomposition method decomposed the five-degree-of freedom turbine loads to reference loading for each actuator. An additional seven-degree-of-freedom dummy load is also incorporated. The system offered significant improvement and increased turbine reliability and high system design confidence. Yin et al. (2017b) proposed a new loading control system to simulate five-degree of freedom load in a wind turbine wherein rotor and blades are replaced by rotating disc and driven by electric motor. A load decomposition-based loading control technique is proposed to decompose loads into reference loading force for each actuator. The system exhibited good accuracy and exhibited high confidence level. A control novel strategy for a megawatt scale wind turbine has been proposed by Yin and his colleagues (Yin et al., 2015a) to improve power efficiency and quality. The system is designed for a hydro-viscous transmission based continuously variable speed wind turbine and a hydro-viscous element is integrated into the turbine drive-train to alleviate the upstream wind-loading fluctuations. The system offered several advantages and improvements such as large power capacity, high efficiency, portable power convertors, and affordability. Yin and colleagues (Yin et al., 2017a) proposed a pitch control system for wind turbines by adopting a practical loading compensation approach that is robust and accurate and smoothens generator power. In the proposed system, a hydraulic motor is used to pitch the turbine blade and augments the accuracy of the system and improves the torque/weight ratio. The pitch control system does not make use of additional sensors making the system cost effective and less complex. Yin (2018) presented a detailed review of continuously variable speed wind turbines (CVSWTs) with variable transmission and reported that improved power efficiency and enhanced power control capabilities could be achieved by adapting mechatronic variable transmissions in the turbine drive train.

Lan et al. (2018) used adaptive SMC to control blade pitch angle and depicted that their control strategy was fault tolerant. Guenoune and his colleagues (Guenoune et al., 2017) studied the

modeling and control of a novel Twin wind turbine (TWT). They implemented SMC to track maximum power. Their results show that SMC exhibited low pitch angle errors, reduced oscillations, reduced fatigue on wind structure, and produced maximum energy. Evangelista and her team (Evangelista et al., 2017) studied SMCs for wind turbine to optimize energy production and found the controller effective in the presence of "model uncertainties and fast disturbances due to gusty wind effects". Tahir and his colleagues (Tahir et al., 2018) have shown that SMC controllers are equipped to handle nonlinearities and randomness in the wind energy conversion systems in the presence of model uncertainties.

Agarwala and Ro (2015, 2013) and Agarwala (2014) focused on the design, evaluation, and analysis of innovative rotor blades for large wind turbines through the formulation of a novel and simple separated pitch control strategy at blade tip (SePCaT) for a large MW wind turbine. The redesigned blade is aerodynamically more effective compared to traditional blade. Deployment of SePCaT facilitated new innovative design whereby a larger portion of the blade was aerodynamically available while maintaining structural effectiveness. The redesigned and improved bladed is more effective when compared to traditional design and maximizes power extraction.

The primary contribution of this research is the design and implementation of a pitch angle control strategy at the outer section of the blade via a separated pitch control at blade tip (SePCaT). A pneumatic actuator is implemented to drive the pitch angle control mechanism by incorporating pneumatic actuated muscles (PAM) due to its high power/mass ratio, high specific work, and good contraction ratio and while maintaining a lighter blade tip. SMC is implemented on the redesigned blade and a novel actuator is deployed on the pitch controller system. A saturation function is used to reduce the chattering behavior of the SMC.

This paper is organized as follows. Section 2 covers mathematical model of blade and blade tip. Wind turbine blade redesign and improvements are covered in Section 3. Mathematical model of the pitch actuator is covered in Section 4. Mathematical model of sliding mode controller is covered in Section 5. Section 6 covers the results. Conclusions are covered in Section 7 followed by references.

Nomenclature

L_s	Lift force (N)
ρ	Density of air (kg/m^3)
U	Wind velocity (m/s)
d	Airfoil chord length for main blade (m)
CL_A	Non-dimensional lift coefficient per angle of attack
dl	Incremental length of the blade (m)
A	Pitch of attack for main blade (rad)
PB_{CA}	Control angle for SePCaT (rad)
h	Plunge (m)
d	Airfoil chord length for main blade (m)
b	Airfoil chord half-length for main blade (m)
l	Length of the blade for main blade (m)
a	Fractional of chord distance between pitch axis (PA) and mid chord (MC)
e	Fractional of chord distance between PA and AC
d_{PB}	Airfoil chord length for SePCaT (m)
d_{PB}	Airfoil chord half-length for SePCaT (m)
l_{PB}	Length of the blade for SepCaT (m)
a_{PB}	Fractional of chord distance btw PA and MC for SePCaT
e_{PB}	Fractional of chord distance btw PA and AC for SePCaT
C_{TH}	Theodorsen's function
CM_A	Moment coefficient per angle of attack

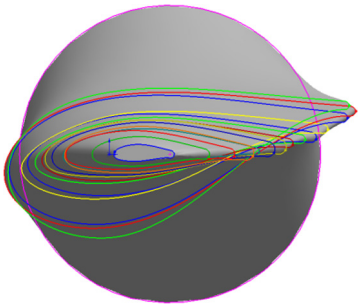

Fig. 1. 3D model of the representative 5 MW wind turbine blade.

CL_A	Lift coefficient per angle of attack
$CMPB_{CA}$	Moment coefficient of SePCaT
$CLPB_{CA}$	Lift coefficient of SePCaT
W	Weight of SePCaT
x_m	Distance of the aerodynamic center from the SePCaT pitching axis (m)
x_g	Distance of the center of gravity from the SePCaT pitching axis (m)
k_{PAM1} & k_{PAM2}	PAM constants
δ_1 & δ_2	PAM deflections
d_{PAM1} & d_{PAM2}	Distances of the PAM line of action to the controller pitching axis (m)
I_s	Moment of inertia of SePCaT (kg m^2)
c_θ	Linear damping term (N m)
$c_{\theta,NL}$	Non-linear damping term (N m)
k_θ	Linear spring stiffness term (N/m)
$k_{\theta,NL}$	Non-linear stiffness term (N/m)
Q_{aero}	Change in aerodynamic moment (N m)
$Q_{control}$	Controller applied moment (N m)
F	Overall PAM actuator force (N)
b	Controller parameter
u	Controller input
$\triangle\delta$	Change in PAM displacement (m)
$\ddot{\theta}$	Angular acceleration (deg/s^2)
$\dot{\theta}$	Angular velocity (deg/s)
θ	Actual/measured angle (deg)
θ_d	SePCaT pitch angle (deg)
$\dot{\theta}_d$	SePCaT pitch angular velocity (deg/s)
$\ddot{\theta}_d$	SePCaT pitch angular acceleration (deg/s^2)
s	Sliding surface
c	Sliding surface constant
e	Error dynamics (deg)
V	Lyapunov function
ε	Constant rate assisting the system to reach the sliding manifold
γ	Constant for saturation function

2. Mathematical model of blade and blade tip

The 3D turbine blade was designed and constructed in a computer aided design (CAD) 3D modeling tool as per the specifications of the NREL 5 MW Wind Turbine (Jonkman et al., 2009) as shown in Fig. 1.

Airfoils at each section are scaled and rotated by their chord lengths and values of angular twists. Various cross-sections were lofted and connected using inbuilt CAD modeling interpolation routines. Complete details of the air foil, the associated data, and 3D modeling details were documented by Agarwala and Ro (2013).

For a small section of blade as per Fig. 2, the aerodynamic forces are given as per Eqs. (1) and (2). The lift force at the aerodynamic center of any blade section is caused due to the pressure difference

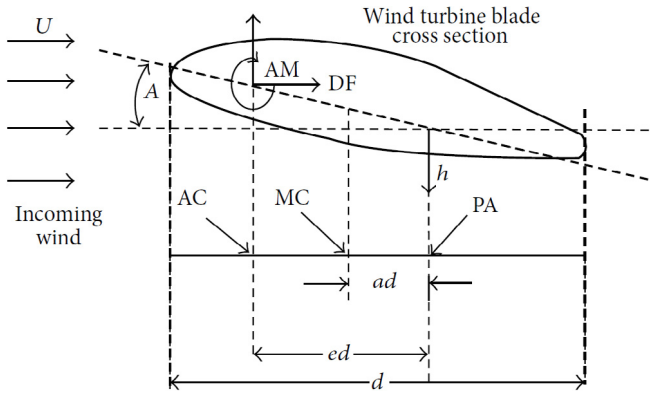

Fig. 2. Cross-section of a wind turbine blade.

between the upper and lower surface of the airfoil when the air flows past that airfoil section.

The lift coefficient is non-dimensional term that captures the geometry of the airfoil impacted by lift forces. Similarly, the aerodynamic moment is computed by multiplying the vertical forces with the chord length. The moment coefficient is a non-dimensional term that captures the geometry of the airfoil impacted by aerodynamic moment.

$$dL = \frac{1}{2}\rho U^2 dCL_A dl + \frac{1}{2}\rho U^2 d_{PB} CL_{PB_{CA}} dl_{PB} \tag{1}$$

$$dM = \frac{1}{2}\rho U^2 d^2 CM_A dl + \frac{1}{2}\rho U^2 {d_{PB}}^2 CM_{PB_{CA}} dl_{PB} \tag{2}$$

The total combined lift and moment for the main blade and SePCaT is obtained by integrating the lift and moment values for the entire blade length exposed to wind and are given in Eqs. (3) and (4).

$$L = \frac{1}{2}\rho U^2 dCL_A \int_0^l dl + \frac{1}{2}\rho U^2 d_{PB} CL_{PB_{CA}} \int_0^{l_{PB}} dl_{PB} \tag{3}$$

$$M = \frac{1}{2}\rho U^2 d^2 CM_A \int_0^l dl + \frac{1}{2}\rho U^2 {d_{PB}}^2 CM_{PB_{CA}} \int_0^{l_{PB}} dl_{PB} \tag{4}$$

The unsteady airfoil moment and lift are dependent on the first and second derivatives of the airfoil plunge, pitch angle of the overall blade and its first and second derivatives, control angle of SePCaT and its first and second derivatives, velocity of air, density of air, and time as shown in Eq. (5).

$$\begin{aligned} L &= L(\dot{h}, \ddot{h}, A, \dot{A}, \ddot{A}, PB_{CA}, \dot{P}B_{CA}, P\ddot{B}_{CA}, U, \rho, time) \\ M &= M(\dot{h}, \ddot{h}, A, \dot{A}, \ddot{A}, PB_{CA}, \dot{P}B_{CA}, P\ddot{B}_{CA}, U, \rho, time) \end{aligned} \tag{5}$$

The total airfoil lift and moment is a combination of steady-state lift due to circulatory motion based on blade pitching, lift due to non-circulatory motion caused by blade pitching and plunging, and lift change due to the pitch, plunge and angular position of the control surface as shown in Eq. (6).

$$\begin{aligned} L &= L_{steady\ state} + L_{circulatory\ motion} + L_{non-circulatory\ motion} \\ &\quad + L_{control\ surface} \\ M &= M_{steady\ state} + M_{circulatory\ motion} + M_{non-circulatory\ motion} \\ &\quad + M_{control\ surface} \end{aligned} \tag{6}$$

The unsteady airfoil lift and moment are based on the unsteady aerodynamic theory (Singh and Yim, 2003; Fung, 2008; Hoogedoorn et al., 2010) as shown in Eqs. (7) and (8).

$$\begin{aligned} L &= \pi\rho b^2(\ddot{h} + U\dot{A} - ba\ddot{A}) \\ &\quad + 2\pi\rho U C_{TH} b\left[\dot{h} + UA + \left(\frac{1}{2} - a\right) b\dot{A}\right] \end{aligned} \tag{7}$$

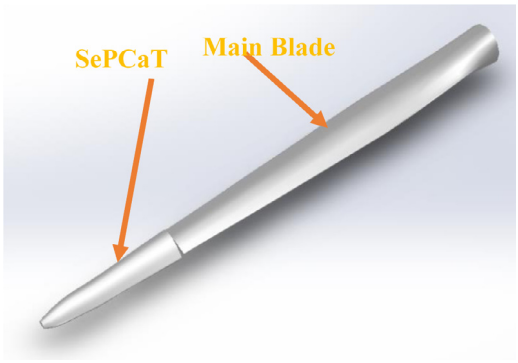

Fig. 3. Main blade and SePCaT.

$$\begin{aligned} M &= -\pi\rho b^3\left[-a\ddot{h} + \left(\frac{1}{2} - a\right) U\dot{A} + \left(\frac{1}{8} - a^2\right) b\ddot{A}\right] + \\ &\quad 2\pi\rho U C_{TH} b^2\left[\left(\frac{1}{2} + a\right)\left(\dot{h} + UA + \left(\frac{1}{2} - a\right)\dot{A}\right)\right] \end{aligned} \tag{8}$$

Agarwala and Ro (2015) proposed on the design, evaluation, and analysis of innovative rotor blades for large wind turbines through the formulation of a novel and simple separated pitch control strategy at blade tip (SePCaT) for a large MW wind turbine.

Deployment of SePCaT as depicted in Fig. 3 facilitated a new design whereby a larger portion of the blade was aerodynamically available while maintaining structural effectiveness thus streamlining blade geometric and structural characteristics. Lift and moment equations with SePCaT deployed as shown in Fig. 3 are depicted in Eqs. (9) and (10). The second term on the right-hand side of the equations represents a contribution due to SePCaT, as indicated in the equations.

$$\begin{aligned} L &= \rho U^2 b C L_A\left[A + \frac{\dot{h}}{U} + \left(\frac{1}{2} - a\right) b\frac{\dot{A}}{U}\right] \\ &\quad + \underbrace{\rho U^2 b_{PB} CL_{PB_{CA}}\left[PB_{CA} + \frac{\dot{h}}{U} + \left(\frac{1}{2} - a_{PB}\right) b_{PB}\frac{P\dot{B}_{CA}}{U}\right]}_{SePCaT} \end{aligned} \tag{9}$$

$$\begin{aligned} M &= \rho U^2 b^2 C M_A\left[A + \frac{\dot{h}}{U} + \left(\frac{1}{2} - a\right) b\frac{\dot{A}}{U}\right] \\ &\quad + \underbrace{\rho U^2 {b_{PB}}^2 CM_{PB_{CA}}\left[PB_{CA} + \frac{\dot{h}}{U} + \left(\frac{1}{2} - a_{PB}\right) b_{PB}\frac{P\dot{B}_{CA}}{U}\right]}_{SePCaT} \end{aligned} \tag{10}$$

Lift and moment equations for exclusive SePCaT actuations reduce to Eqs. (11) and (12).

$$\begin{aligned} L_S &= \rho U^2 b C L_A\left[A + \frac{\dot{h}}{U}\right] + \\ &\quad \rho U^2 b_{PB} CL_{PB_{CA}}\left[PB_{CA} + \frac{\dot{h}}{U} + \left(\frac{1}{2} - a_{PB}\right) b_{PB}\frac{P\dot{B}_{CA}}{U}\right] \end{aligned} \tag{11}$$

$$\begin{aligned} M_S &= \rho U^2 b^2 C M_A\left[A + \frac{\dot{h}}{U}\right] + \\ &\quad \rho U^2 {b_{PB}}^2 CM_{PB_{CA}}\left[PB_{CA} + \frac{\dot{h}}{U} + \left(\frac{1}{2} - a_{PB}\right) b_{PB}\frac{P\dot{B}_{CA}}{U}\right] \end{aligned} \tag{12}$$

3. Wind turbine blade redesign and improvement

The goal of the redesigned blade was to make larger portion of the blade available for aerodynamic effectiveness. Agarwala and Ro (2015, 2013) and Agarwala (2014) focused on a simple separated pitch control strategy at blade tip (SePCaT) for a large

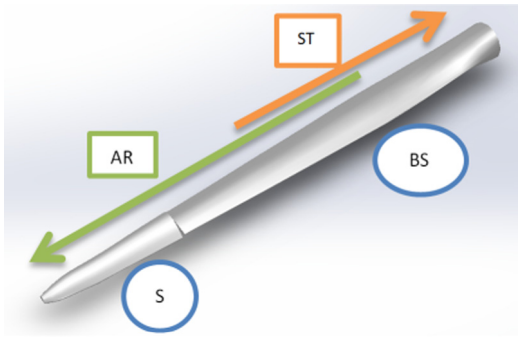

Fig. 4. Regions of aerodynamic (AR) and structural regions (ST)-Original Blade.

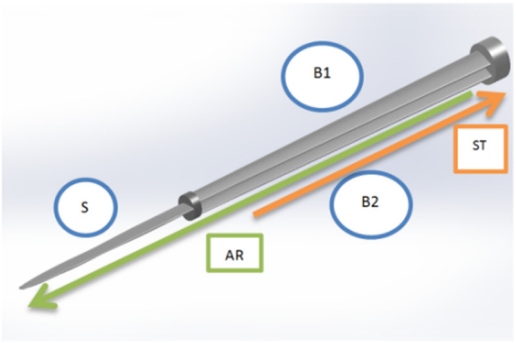

Fig. 5. Regions of aerodynamic (AR) and structural regions (ST)- redesigned blade.

MW wind turbine. The root of the traditional blade is much thicker to withstand high stresses arising from blade loads. These stresses are more pronounced during high speeds during when the entire blade is actively pitched to limit power so that they operate within the safe material stress limits of the wind turbine blade. In current wind turbine blades, part of the blade's mid-span and the tip contribute to a majority of the aerodynamic effectiveness needed by the rotor for power extraction. Fig. 4 depicts the allocated regions of blade aerodynamic (AR) and structural regions (ST) for the traditional blade with SePCaT. BS refers to the main blade and S to SePCaT. Traditional blade combined with SePCaT has its limitations due to large blade weight and a larger portion of the blade that is less aerodynamically effective.

The redesigned blade (see Fig. 5) is comprised of two inner blades (B1, B2). B1 and B2 use a thinner airfoil configuration near the root and maintain their blade stiffness by means of a combination of two parallel stiffness elements to withstand higher stresses. As a result, the entire blade along with the root is aerodynamically more effective when compared the traditional design and more power can be extracted.

The blades (B1 and B2) were optimized for their respective pitch angle settings (Agarwala and Ro, 2015). The pitch angle of 24 degrees for the upper blade and 25 degrees for the lower blade produced the maximum lift forces. Lateral sizes of the inner blades B1 and B2 at 50 percent of blade BS; and lengths of B1 and B2 at 80 percent of BS have similar aerodynamic effectiveness when compared to BS. It was also observed that 1.5 m gap between B1 and B2; B1 at an angle of 24 degrees; B2 at an angle of 25 degrees; and S at an angle of 25 degrees has the optimum aerodynamic effect. However, analysis was not conducted to prove that the aerodynamically effective blade was structurally compliant. CFD analysis and results of the redesigned blade was reported in Agarwala and Ro (2015).

4. Mathematical model of pitch actuator

Traditional motor-based pitch control pitch controllers are heavy and therefore not suitable for deployment on the redesigned wind turbine blade with SePCaT. The goal of the actuator design is to keep them as light as possible while exhibiting strong actuator force. A novel approach is adopted where Pneumatically Actuated Muscles (PAM) is used for actively pitching the wind turbine blade. PAMS are very light and have a high specific work and a good contraction ratio. Readers are encouraged to refer to the work Woods and his colleagues (Woods et al., 2011b,a, 2014) to learn more about PAM, its structure, and theory. To pitch the blade, PAM or clusters of PAM are used. As depicted in Figs. 6 and 7 (next page), PAM combinations 1 and 2, when actuated, allow the SePCaT to be pitched to feather while PAMs 3 and 4, when actuated, allow the SePCaT to be pitched to stall.

In Fig. 7 (next page), the free body diagram of the controller is shown. The SePCaT cross-sectional view inside the connector which is acted upon by the PAM is also shown.

The equation of motion of actuator as per Figs. 6, 7 and PAM model is shown below.

$$I_s\ddot{\theta} + k_\theta\theta + k_{\theta,NL}\theta^3 + \left(c_\theta\dot{\theta} + c_{\theta,NL}sign\left(\dot{\theta}\right)\right) = Q_{aero} + Q_{control} \tag{13}$$

As shown below, the PAM actuator force is expressed in terms of the overall PAM actuator force, deflection and PAM constant. Both PAMs have same geometrical and dynamical properties.

$$F = k_{PAM}\delta \tag{14}$$

The relationship between Q_{aero} and $Q_{control}$ is shown below.

$$2k_{PAM} * \triangle\delta * d_{PAM} - Q_{aero} = Q_{control} \tag{15}$$

where d_{PAM} is the distance of the PAM line of action to the SePCaT pitching axis and $\triangle\delta$ is the change in PAM displacement.

Therefore Eq. (4) becomes

$$I_s\ddot{\theta} + k_\theta\theta + k_{\theta,NL}\theta^3 + \left(c_\theta\dot{\theta} + c_{\theta,NL}sign\left(\dot{\theta}\right)\right) = 2k_{PAM} * \triangle\delta * d_{PAM} \tag{16}$$

Finally, Eq. (17) is obtained by expressing equation (16) as functions of θ, controller input u and parameter b as shown below.

$$\ddot{\theta} = -f(\theta) + bu \tag{17}$$

where,

$$f(\theta) = \frac{c_\theta\dot{\theta}}{I_s} + \frac{c_{\theta,NL}sign\left(\dot{\theta}\right)}{I_s} + \frac{k_\theta\theta}{I_s} + \frac{k_{\theta,NL}\theta^3}{I_s}$$

$$b = \frac{2k_{PAM}d_{PAM}}{I_s}$$

$$u = \triangle\delta = \delta_u$$

5. Mathematical model of sliding mode controller

A SMC controller is envisaged. Readers are encouraged to refer to the book by Liu and his colleagues (Liu and Wang, 2012) to learn more about SMC. Governing equations for the SMC is derived as follows.

A sliding surface be selected such that

$$s = \dot{e} + ce, \quad c > 0 \tag{18}$$

Here e the error dynamics while c is a constant. The definition of e is as follows.

$$e = \theta_d - \theta \tag{19}$$

where the desired SePCaT pitch angle is θ_d and the actual/measured angle is θ.

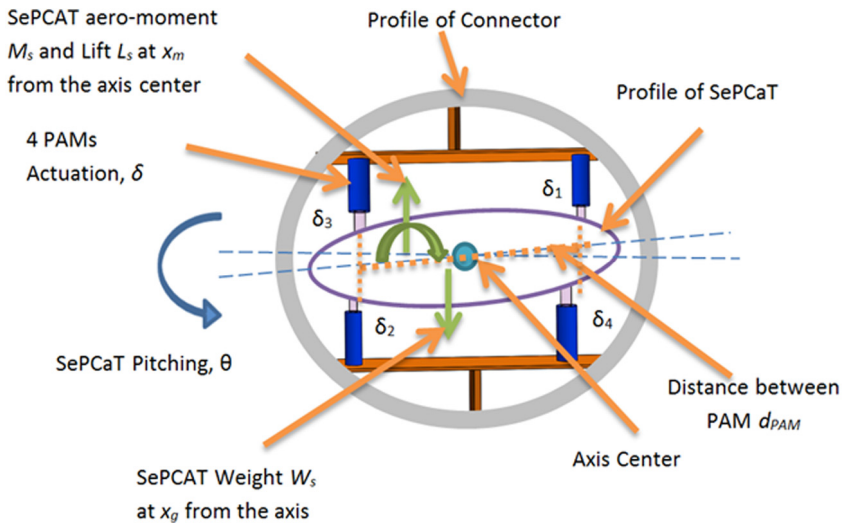

Fig. 6. Pitch controller enabled by PAM.

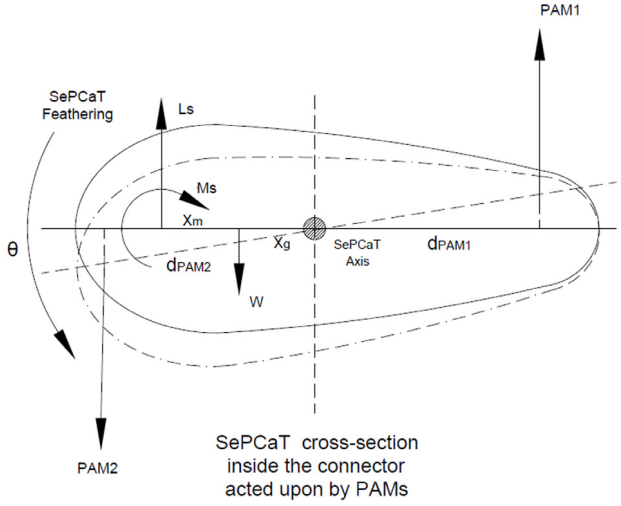

Fig. 7. Free body diagram of the Controller.

A Lyapunov function V is selected and defined as shown.

$$V = \frac{1}{2}s^2 > 0 \tag{20}$$

Here s is a sliding surface. For stability, the Lyapunov function must be positive definite and its derivative must be negative-definite as follows.

$$\dot{V} = s\dot{s} < 0 \tag{21}$$

Expressing s in terms of the error dynamics

$$s = \left(\dot{\theta}_d - \dot{\theta}\right) + c\left(\theta_d - \theta\right) \tag{22}$$

The derivative of s is given as

$$\dot{s} = \left(\ddot{\theta}_d - \ddot{\theta}\right) + c\left(\dot{\theta}_d - \dot{\theta}\right) \tag{23}$$

Rearranging the terms and incorporating the system dynamics, we have the following.

$$\dot{s} = \left(\ddot{\theta}_d + f\left(\theta\right) - bu\right) + c\left(\dot{\theta}_d - \dot{\theta}\right) \tag{24}$$

In terms of the controller input u, the above expression can be recast as follows.

$$u = \frac{1}{b}\left[f\left(\theta\right) + \ddot{\theta}_d + c\left(\dot{\theta}_d - \dot{\theta}\right) - \dot{s}\right] \tag{25}$$

A constant rate reaching law is selected as shown below.

$$\dot{s} = -\varepsilon\, sgn\left(s\right),\ \varepsilon > 0 \tag{26}$$

Here ε is the constant rate which helps the systems reach the sliding manifold. The above equation shows that $\dot{V}$ is negative semi-definite. Therefore, the final control law for the system is as shown below.

$$u = \frac{1}{b}\left[f\left(\theta\right) + \ddot{\theta}_d + c\left(\dot{\theta}_d - \dot{\theta}\right) + \varepsilon\, sgn\left(s\right)\right] \tag{27}$$

6. Results

6.1. Desired pitch angle control trajectories

The desired trajectory for SePCaT pitch angle in response to power abatement (shed excessive power to maintain 5 MW) in region 3 is discussed in Agarwala and Ro (2015). SePCaT configurations, varied from 5 to 30% of the blade length in 5% increments (SePCaT5, SePCaT10, SePCaT15, SePCaT20, SePCaT25, and SePCaT30), are evaluated by comparing them to aero-dynamical responses of the traditional blade. As the wind speed increases by a factor of 1.1U (10 percent), the rotor power increases to around 6.75 MW warranting its reduction to a factor of .74 approximately. This is achieved by feathering SePCaT30 by 14, SePCaT25 by 16, SePCaT20 by 26, and SePCaT15 by 30 degrees respectively. If wind speed increases by a factor of 1.2U (20 percent), the rotor power increases to around 8.33 MW warranting its reduction to a factor of.6 approximately. This is achieved by feathering SePCaT30 by 18, SePCaT25 by 26 and SePCaT20 by 30 degrees respectively. As the wind speed increases by a factor of 1.3U (30 percent), the rotor power increases to around 11.75 MW warranting its reduction to a factor of .43 approximately. This is achieved by feathering SePCaT30 by 26 degrees. If wind speed increases by a factor of 1.4U (40 percent), the rotor power increases to around 14.30 MW warranting its reduction to a factor of .35 approximately. This is achieved by feathering SePCaT30 by 32 degrees. The settings in Table 1 are used to build the desired SePCaT pitch angle trajectory for power shedding. Fig. 8 depicts both the signals (top portion is Signal 1 and bottom portion is Signal 2) used for desired pitch angle trajectories.

SMC is subjected to desired pitch angle trajectories and the robustness of their responses are observed.

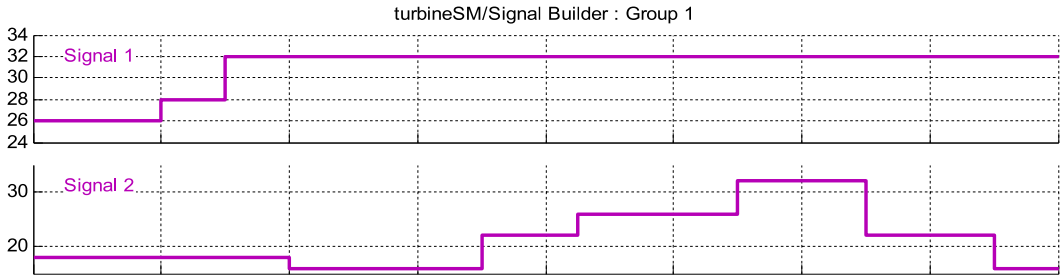

Fig. 8. Desired trajectory for SePCaT pitch angle in response to power abatement.

Table 1
SePCaT pitch angle trajectory setup values for desired pitch signals.

Wind speed factor	Power produced	Rated power	SePCaT30 angle (°)	SePCaT25 angle (°)	SePCaT20 angle (°)	SePCaT15 angle (°)
1.1	6.75 MW	5 MW	14	16	26	30
1.2	8.33 MW	5 MW	18	26	30	–
1.3	11.75 MW	5 MW	26	–	–	–
1.4	14.30 MW	5 MW	32	–	–	–

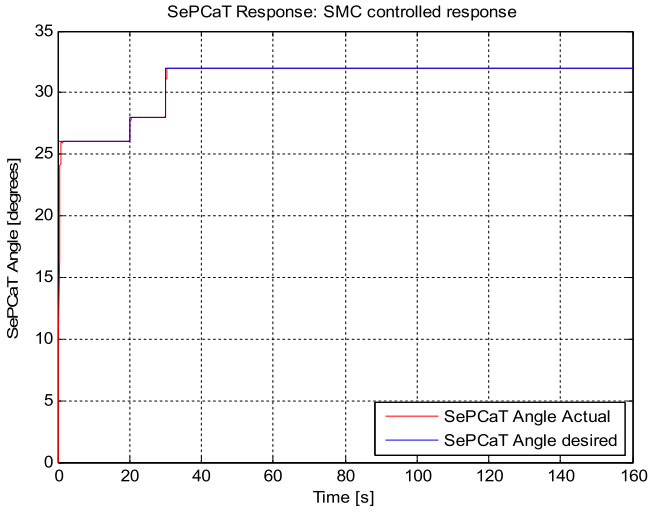

Fig. 9. SMC response for signal 1.

6.2. SMC numerical results

SMC is deployed on the wind turbine and the values of ε and c in the SMC control law (Eq. (27)) are iterated to achieve a satisfactory pitch error. It is observed that $\varepsilon = 6$, $c = 8$ yield satisfactory tracking as depicted in Figs. 9 through 12. Fig. 9 indicates the SMC controller tracking response to signal 1 and Fig. 10 (next page) indicates the pitch angle error. It is evident from Fig. 10 that the maximum SMC pitch angle error during operation of the wind turbine is around .002 degrees.

Fig. 11 (next page) indicates the SMC controller tracking response to signal 2 and Fig. 12 (on page 19) indicates the resulting pitch angle error. It is evident from Fig. 12 that the maximum pitch angle error during most of the operation of the wind turbine around 0.003 degrees.

6.3. Performance and robustness improvements of SMC

Examination of signal 1 for sliding mode reveals chattering behavior as depicted by the zoomed-in curve of Fig. 9 and as depicted in Fig. 13.

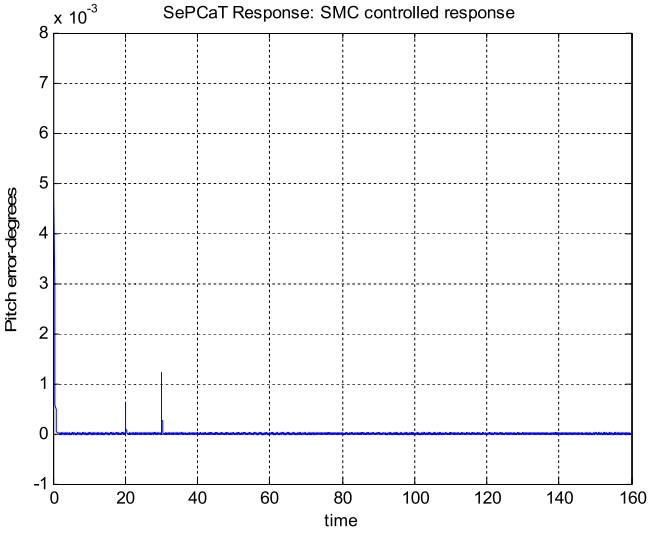

Fig. 10. Pitch angle error when SMC is deployed for signal 1.

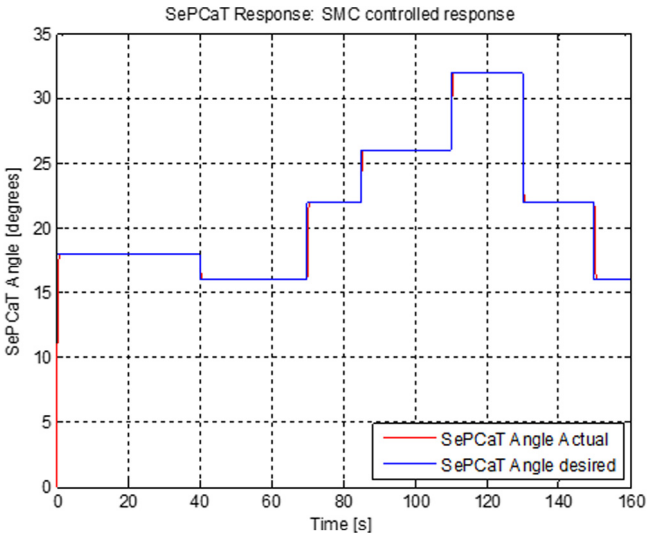

Fig. 11. SMC response for signal 2.

This chattering behavior leads to actuator vibration and shortening of actuator life. To minimize this chattering behavior a saturation function is used instead of the sign function as shown below.

The reaching law is selected as

$$\dot{s} = -\varepsilon\, sat\,(s, \gamma)\,,\ \varepsilon > 0 \tag{28}$$

The saturation signal is defined as

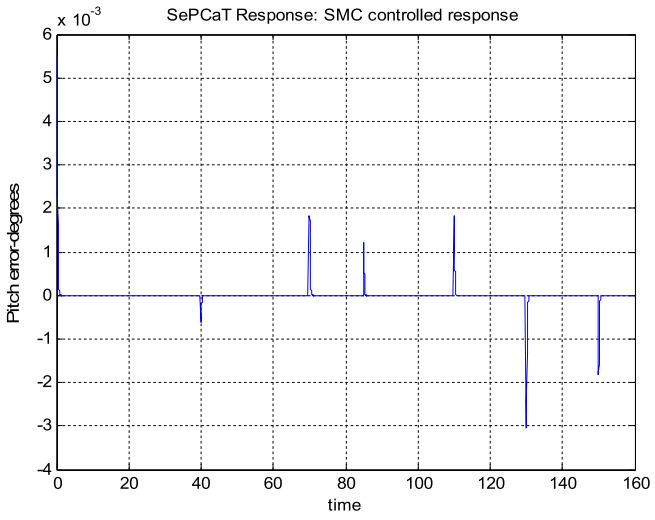

Fig. 12. Pitch error when SMC is deployed for signal 2.

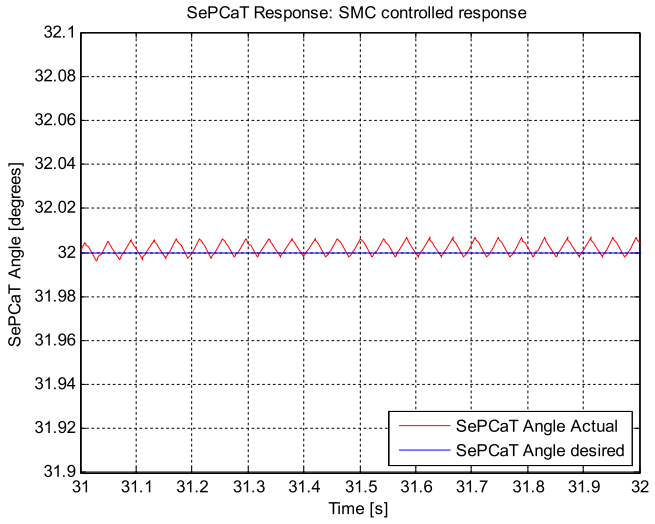

Fig. 13. Chattering when SMC ε *sgn* (s) is deployed.

$$sat\ (s, \gamma) = \begin{cases} 1 & s > \gamma \\ \dfrac{s}{\gamma} & -\gamma \leq s \leq \gamma \\ -1 & s < -\gamma \end{cases} \tag{29}$$

The final control law is then given as

$$u = \frac{1}{b}\left[f\ (\theta) + \ddot{\theta}_d + c\left(\dot{\theta}_d - \dot{\theta}\right) + \varepsilon\ sat\ (s, \gamma)\right] \tag{30}$$

The values of γ are chosen to alter the slope of the saturation function and the results are observed. It is observed that chattering is minimized at larger values of the slope. It is observed that changing the value of γ from .1 to .001 reduces the chatter from around .01 degrees to negligible and results in smoother trajectory tracking and SMC robustness as depicted in Figs. 14, 15, and 16.

7. Conclusion

In this paper a pitch angle control strategy was designed and implemented at the outer section of the blade via a separated

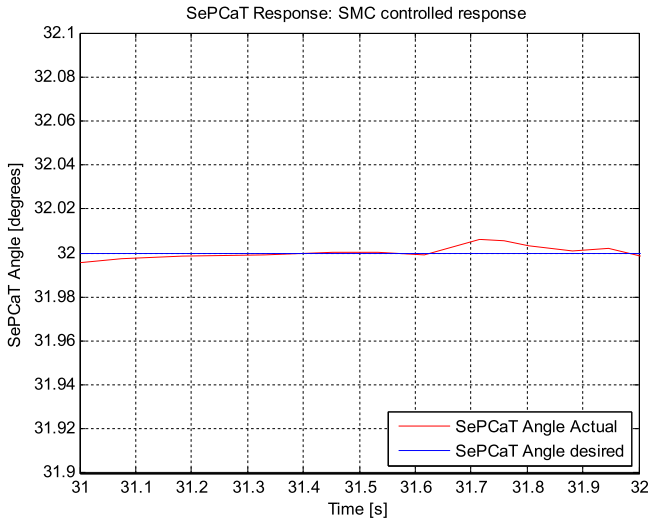

Fig. 14. Chattering reduction when SISO SMC ε *sat* (s, γ) is deployed. The value of γ is .1.

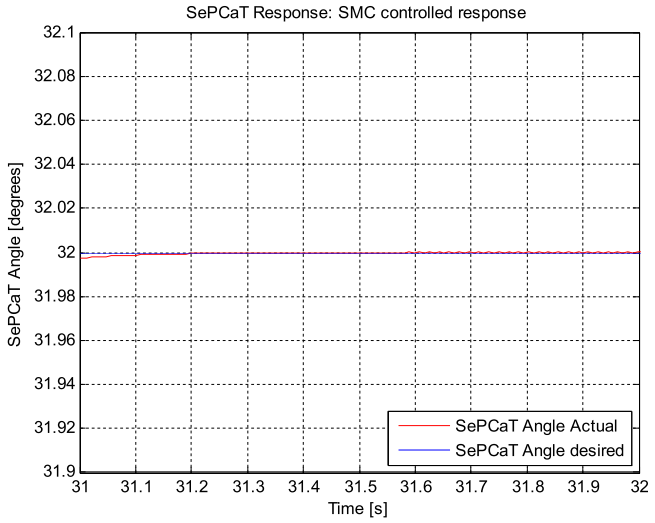

Fig. 15. Chattering reduction when SISO SMC ε *sat* (s, γ) is deployed. The value of γ is .01.

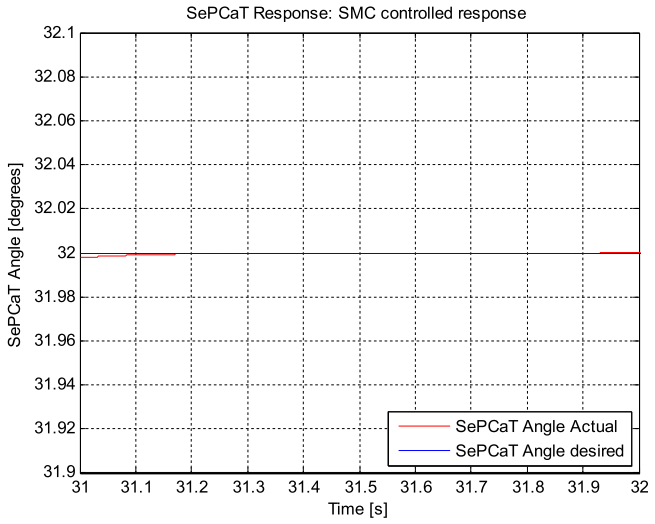

Fig. 16. Chattering reduction when SISO SMC ε *sat* (s, γ) is deployed. The value of γ is .001.

pitch control at blade tip (SePCaT). A pneumatic actuator was deployed to drive the pitch angle control mechanism by incorporating pneumatic actuated muscles (PAM) due to its high power/mass ratio, high specific work, and good contraction ratio and a sliding mode controller (SMC) algorithm. The control strategy was implemented on a redesigned 5 MW wind turbine blade. A saturation function was used to reduce the chattering behavior of the SMC. Several pitch angle trajectories signals were generated, the numerical responses were observed and compared, and the following findings are made, (1) It was observed that the maximum pitch angle error during majority of the wind turbine trajectory was around 0.003 degrees.; (2) Although SMC exhibited satisfactory pitch angle tracking, investigation and closer look of controller response revealed chattering behavior. Chattering characteristics leads to actuator vibration and shortening of actuator life; (3) To minimize this chattering behavior, a saturation function was used as the reaching law for the SMC. The values γ was chosen to alter the slope of the saturation function and the results are further observed; (4) It is observed that varying the value of γ from .1 to .001 reduces the chattering magnitude from .01 degrees to almost negligible and results in smoother trajectory tracking and improved controller robustness.

SePCaT is the pitch control of a shorter blade length at the tip and the pitch controller incorporating PAM and SMC offers a significant advantage over traditional full-length control.

More work is anticipated in the future. These studies were carried out in numerically and hence the authors plan to conduct experimental validation of the work in the futures. In the future, other novel pitch control strategies inspired by research by Yin et al. (2015f,g, 2016a) and control techniques such as adaptive sliding mode back-stepping pitch angle control can be implemented on SePCaT.

References

Agarwala, R., 2014. Separated Pitch Control at Tip (SePCaT): A Novel Blade Design and Associated Control Strategies for Large MW Wind Turbines. North Carolina State University.

Agarwala, Ranjeet, Ro, Paul I., 2013. 3d analysis of lift and moment adaptation via control surface deployments on a 5 MW Wind Turbine Blade. Wind Eng. 37 (5), 447–468.

Agarwala, Ranjeet, Ro, Paul I., 2015. Separated pitch control at tip (sepcat): innovative blade design explorations for large mw wind turbine blades. J. Wind Energy.

Evangelista, CA., Pisano, A., Puleston, P., Usai, E., 2017. Receding horizon adaptive second-order sliding mode control for doubly-fed induction generator based wind turbine. IEEE Trans. Control Syst. Technol. 25 (1), 73–84.

Fung, YC., 2008. An Introduction to the Theory of Aeroelasticity. Courier Dover Publications.

Guenoune, I., Plestan, F., Chermitti, A., Evangelista, C., 2017. Modeling and robust control of a twin wind turbines structure. Control Eng. Practice 69, 23–35.

Hoogedoorn, E., Jacobs, GB., Beyene, A., 2010. Aero-elastic behavior of a flexible blade for wind turbine application: a 2d computational study. Energy. 35 (2), 778–785.

Hu, Y., Chen, MZ., Li, C., 2017. Active structural control for load mitigation of wind turbines via adaptive sliding-mode approach. J. Franklin Inst. 354 (11), 4311–4330.

Jonkman, J., Butterfield, S., Musial, W., Scott, G., 2009. Definition of a 5-MW Reference Wind Turbine for Offshore System Development. National Renewable Energy Lab.(NREL), Golden, CO (United States).

Lan, J., Patton, RJ., Zhu, X., 2018. Fault-tolerant wind turbine pitch control using adaptive sliding mode estimation. Renewable Energy. 116, 219–231.

Liu, J., Wang, X., 2012. Advanced Sliding Mode Control for Mechanical Systems: Design, Analysis and MATLAB Simulation. Springer Science & Business Media.

Singh, SN., Yim, W., 2003. State feedback control of an aeroelastic system with structural nonlinearity. Aerosp. Sci. Technol. 7 (1), 23–31.

Tahir, K., Belfedal, C., Allaoui, T., Denaï, M., Doumi, MH., 2018. A new sliding mode control strategy for variable−speed wind turbine power maximization. Int. Trans. Electr. Energy Syst. e2513.

Woods, BK., Kothera, CS., Sirohi, J., Wereley, NM., 2011a. Pneumatic artificial muscles for trailing edge flap actuation: a feasibility study. Smart Mater. Struct. 20 (10), 105021.

Woods, BK., Kothera, CS., Wereley, NM., 2011b. Wind tunnel testing of a helicopter rotor trailing edge flap actuated via pneumatic artificial muscles. J. Intell. Mater. Syst. Struct. 22 (13), 1513–1528.

Woods, BK., Kothera, CS., Wereley, NM., 2014. Whirl testing of a pneumatic artificial muscle actuation system for a full-scale active rotor. J. Am. Helicopter Soc. 59 (2), 1-1.

Yang, B., Yu, T., Shu, H., Dong, J., Jiang, L., 2018a. Robust sliding-mode control of wind energy conversion systems for optimal power extraction via nonlinear perturbation observers. Appl. Energy. 210, 711–723.

Yang, B., Yu, T., Shu, H., Zhang, Y., Chen, J., Sang, Y., Jiang, L., 2018b. Passivity-based sliding-mode control design for optimal power extraction of a pmsg based variable speed wind turbine. Renewable Energy. 119, 577–589.

Yin, X., 2018. An up to date review of continuously variable speed wind turbines with mechatronic variable transmissions. Int. J. Energy Res. 2542 (4), 1442–1454.

Yin, XX., Lin, YG., Li, W., 2015a. Operating modes and control strategy for megawatt-scale hydro-viscous transmission-based continuously variable speed wind turbines. IEEE Trans. Sustainable Energy 6 (4), 1553–1564.

Yin, XX., Lin, YG., Li, W., 2016a. Predictive pitch control of an electro-hydraulic digital pitch system for wind turbines based on the extreme learning machine. Trans. Inst. Measur. Control 38 (11), 1392–1400.

Yin, XX., Lin, YG., Li, W., 2017a. Modeling and loading compensation of a rotary valve-controlled pitch system for wind turbines. J. Zhejiang Univ.-Sci. A. 18 (9), 718–727.

Yin, XX., Lin, YG., Li, W., Gu, YJ., 2014a. Integrated pitch control for wind turbine based on a novel pitch control system. J. Renew. Sustainable Energy. 6 (4), 043106.

Yin, XX., Lin, YG., Li, W., Gu, HG., 2016b. Hydro-viscous transmission based maximum power extraction control for continuously variable speed wind turbine with enhanced efficiency. Renewable Energy. 87, 646–655.

Yin, XX., Lin, YG., Li, W., Gu, YJ., Lei, PF., Liu, HW., 2015b. Adaptive back-stepping pitch angle control for wind turbine based on a new electro-hydraulic pitch system. Int. J. Control 88 (11), 2316–2326.

Yin, XX., Lin, YG., Li, W., Gu, YJ., Lei, PF., Liu, HW., 2015c. Sliding mode voltage control strategy for capturing maximum wind energy based on fuzzy logic control. Int. J. Electr. Power Energy Syst. 70, 45–51.

Yin, XX., Lin, YG., Li, W., Gu, YJ., Liu, HW., Lei, PF., 2015d. A novel fuzzy integral sliding mode current control strategy for maximizing wind power extraction and eliminating voltage harmonics. Energy. 85, 677–686.

Yin, XX., Lin, YG., Li, W., Gu, YJ., Wang, XJ., Lei, PF., 2015e. Design, modeling and implementation of a novel pitch angle control system for wind turbine. Renewable Energy. 81, 599–608.

Yin, XX., Lin, YG., Li, W., Liu, HW., Gu, YJ., 2014b. Output power control for hydro-viscous transmission based continuously variable speed wind turbine. Renewable energy. 72, 395–405.

Yin, XX., Lin, YG., Li, W., Liu, HW., Gu, YJ., 2015f. Adaptive sliding mode back-stepping pitch angle control of a variable-displacement pump-controlled pitch system for wind turbines. ISA Trans. 58, 629–634.

Yin, XX., Lin, YG., Li, W., Liu, HW., Gu, YJ., 2015g. Fuzzy-logic sliding-mode control strategy for extracting maximum wind power. IEEE Trans. Energy Conversion. 30 (4), 1267–1278.

Yin, XX., Lin, YG., Li, W., Ye, HY., 2017b. Loading system and control strategy for simulating wind turbine loads. J. Vib. Control 23 (11), 1739–1752.

Yin, XX., Lin, YG., Li, W., Ye, HY., Gu, YJ., Liu, HW., 2015. Reproduction of five degree-of-freedom loads for wind turbine using equispaced electro-hydraulic actuators. Renewable Energy. 83, 626–637.